

Two Algorithms for Excited-State Quantum Solvers: Theory and Application to EOM-UCCSD

Published as part of *The Journal of Physical Chemistry* virtual special issue "Physical Chemistry of Quantum Information Science".

Yongbin Kim* and Anna I. Krylov*



Cite This: *J. Phys. Chem. A* 2023, 127, 6552–6566



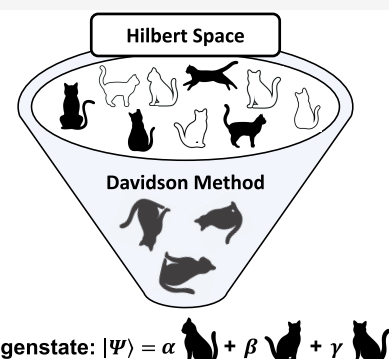
Read Online

ACCESS |

Metrics & More

Article Recommendations

ABSTRACT: Near-term quantum devices promise to revolutionize quantum chemistry, but simulations using the current noisy intermediate-scale quantum (NISQ) devices are not practical due to their high susceptibility to errors. This motivated the design of NISQ algorithms leveraging classical and quantum resources. While several developments have shown promising results for ground-state simulations, extending the algorithms to excited states remains challenging. This paper presents two cost-efficient excited-state algorithms inspired by the classical Davidson algorithm. We implemented the Davidson method into the quantum self-consistent equation-of-motion unitary coupled-cluster (q-sc-EOM-UCC) excited-state method adapted for quantum hardware. The circuit strategies for generating desired excited states are discussed, implemented, and tested. We demonstrate the performance and accuracy of the proposed algorithms (q-sc-EOM-UCC/Davidson and its variational variant) by simulations of H₂, H₄, LiH, and H₂O molecules. Similar to the classical Davidson scheme, q-sc-EOM-UCC/Davidson algorithms are capable of targeting a small number of excited states of the desired character.



I. INTRODUCTION

Quantum computing promises to deliver new technology for solving complex problems that are beyond the capability of conventional classical computers.^{1–6} Particularly exciting is the potential use of quantum computing in quantum chemistry. Electronic structure calculations provide fundamental information about matter and are essential for research in chemistry, physics, and materials science. Unfortunately, the computational complexity of finding the exact solution of the electronic Schrödinger equation scales factorially with the system size, limiting predictive power of quantum chemistry. This unfavorable scaling arises because of the quantum entanglement of the electronic degrees of freedom in many-body wavefunctions. Because the wavefunction is a quantum object, one may expect that it could be encoded on a quantum device more effectively than on classical devices;¹ however, the exact details of effective quantum algorithms for solving the electronic Schrödinger equation remain elusive.

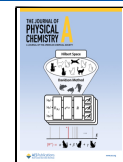
The main task of an electronic structure calculation is finding the eigenvalues of a given molecular Hamiltonian (i.e., electronic energies). One practical quantum algorithm for molecular simulations is called the quantum phase estimation (QPE) algorithm.⁷ QPE—a quantum algorithm for evaluating eigenvalues of a Hermitian operator $\hat{\mathcal{H}}$ —was expected to lead to an exponential speed-up of quantum simulation relative to

classical algorithms. However, a disturbing feature of QPE is the large number of quantum operations that are needed to achieve the target precision: $O(p^{-1})$ successive operations of $e^{i\hat{\mathcal{H}}t}$ are needed for precision p . To execute this operation, each of $e^{i\hat{\mathcal{H}}t}$ is decomposed into millions or billions of quantum gates, which exceeds the capability of noisy intermediate-scale quantum (NISQ) devices.^{8–11} Consequently, although QPE is an important milestone in quantum computing for quantum simulations, it is not practical for realistic applications.¹² To address this limitation, a more NISQ-friendly algorithm with low circuit depths, called a variational quantum eigensolver (VQE), was proposed.¹³ The VQE is a hybrid quantum-classical algorithm based on a variational principle. The algorithm entails preparing a parameterized quantum state on the quantum device and measuring the expectation value of the Hamiltonian on the trial state. The classical optimization procedure iteratively adjusts the parameters of the trial state to minimize the

Received: April 13, 2023

Revised: June 29, 2023

Published: July 28, 2023



expectation value of the Hamiltonian. By leveraging classical optimization techniques with quantum measurements, VQE requires significantly smaller quantum resources compared to QPE. The VQE algorithm has been successfully deployed in ground-state simulations of small molecules on NISQ devices^{13–18} and is exploited in many algorithms for quantum molecular simulations.

The progress in the development of quantum algorithms with shallow circuit depths has enabled successful simulations of molecular ground-state energies. Many applications (e.g., spectroscopy, photochemistry) require going beyond ground-state calculations and computing excited states. The development of quantum algorithms for molecular excited states is more challenging compared to the ground-state algorithms. The existing quantum algorithms for excited states often require a large number of qubits and gate operations, which precludes their application to larger systems. This is because excited states often have more complex wavefunctions (open-shell, multi-configurational) even when the corresponding ground state is well behaved. Furthermore, in contrast to the ground state (which is unique in the sense that it is the lowest-energy state), there are many excited states, so the quantum algorithms should be capable of targeting a specific state (or states)—e.g., the lowest-energy states or states in a particular energy range, states of a particular symmetry/spin, states of a particular character, etc.

The success of the VQE algorithm for ground-state calculations has inspired extensions to excited states, leading to variational quantum deflation (VQD),¹⁹ subspace-search VQE (SSVQE),²⁰ and other algorithms.^{21–24} The underlying framework of all VQE-based methods is the variational principle. The VQE-based methods for excited states employ supplementary constraints so that the resulting algorithms look for a minimum-energy state orthogonal to the previously computed states. For example, the central element of VQD¹⁹ is the penalty terms in the cost function (which is subject to minimization). The penalty terms quantify the overlap between the previously obtained solutions and the current target state. The minimization of the VQD cost function¹⁹ ensures the mutual orthogonality of the computed eigenstates. Thus, the algorithm entails sequential calculations of the states. Importantly, these approaches do not guarantee resolving the full energy spectrum of the Hamiltonian, especially for near-degenerate states. The essential feature of VQE-based approaches is the need to design the ansatz that effectively differentiates each eigenstate of the Hamiltonian from other states.

In the classical quantum chemistry, calculation of excited states is also challenging.^{25–28} Among popular wavefunction-based approaches is the equation-of-motion coupled-cluster (EOM-CC) ansatz.^{28–31} In the complete many-body limit (i.e., when up to N -electron excitations are included), EOM-CC becomes identical to full configuration interaction (FCI)—the exact solution in the given one-electron basis set. In the case of the truncated many-electron basis, EOM-CC is superior to CI due to the incorporation of correlation through a similarity transformation, which also makes the method size-intensive. Quantum adaptations of the EOM ansatz (qEOM) have been implemented and tested.^{32–34} In contrast to the standard EOM-CC, the reference wavefunction of its quantum counterpart comes from the ground-state VQE calculation with the unitary coupled-cluster (UCC) ansatz.³⁵ UCC framework is Hermitian, provides an upper bound for the energy, and is size-extensive by construction. However, the price paid for the variational bound

is that the originally proposed qEOM³² ansatz does not satisfy the killer condition,^{36–38} which ensures the ground state cannot be deexcited. Mukherjee and co-workers proposed a unitary transformation of the EOM projection operators to address the killer condition issue of the UCC theory.^{37,39} Asthana et al.⁴⁰ have implemented this technique^{37,39} on quantum devices. The algorithm, named the quantum self-consistent EOM (q-sc-EOM) method,⁴⁰ yields more accurate excitation energies (EEs), ionization potentials (IPs), and electron affinities (EAs) than the originally proposed qEOM.³²

The q-sc-EOM (and qEOM) procedure leverages classical and quantum computing resources. Specifically, the Hamiltonian matrix is measured on a quantum computer within a given many-electron basis, and the resulting matrix is subsequently diagonalized on a classical computer. Although the measurement processes of the Hamiltonian can potentially benefit from the quantum architecture, for the entire calculation to be effective, one also needs a cost-efficient algorithm for the diagonalization step done on a classical computer. In classical electronic structure calculations, the diagonalization is accomplished through iterative determination of only a few eigenvalues using the Davidson algorithm.^{41–44} The focus of this paper is on the adaptation of the Davidson procedure for quantum computations and its implementation within the q-sc-EOM protocol, which we call the q-sc-EOM-UCC/Davidson algorithm. The key feature of the Davidson implementation on quantum devices is the design of a unitary ansatz that generates specific quantum superposition states, which is achieved by using Gray code decomposition.^{45,46} The proposed ansatz enables targeting a specific subspace within the Hilbert space based on the feedback from the Davidson procedure. Hence, instead of computing the entire spectrum of the Hamiltonian, our q-sc-EOM-UCCSD/Davidson algorithm is capable of computing several transitions of a particular type by defining suitable subspace vectors. Here, we focus on finding low-lying states of a given symmetry/spin, but the algorithm can be easily extended⁴⁴ to finding states around the specified energy or of a particular type (e.g., such as excitations between specific orbitals).

The structure of the paper is as follows: Section II.I discusses EOM formalism, Section II.II describes the choice of the ground-state ansatz for quantum computing and its incorporation within the EOM, Section II.III explains the Davidson procedure with q-sc-EOM implemented on quantum devices, Section II.IV presents the detailed circuit design, and Section II.V presents the variational extension of the proposed algorithm. Section II.VI provides computational details of illustrative calculations and Section III presents the numerical results using a set of small molecules (H_2 , H_4 , LiH, and H_2O). Section IV gives our concluding remarks.

II. METHODS: THEORY

II.I. Equation-of-Motion (EOM) Formalism. The EOM formalism employs projection operators \hat{O}_k that generate target states $|\Psi_k\rangle$ from a reference state $|\Psi_0\rangle$.^{25,47–50} The projection operator \hat{O}_k for a k th excited state of the electronic Hamiltonian is

$$\begin{aligned}\hat{O}_k|\Psi_0\rangle &= |\Psi_k\rangle\langle\Psi_0|\Psi_0\rangle = |\Psi_k\rangle \\ \hat{O}_k^\dagger|\Psi_k\rangle &= |\Psi_0\rangle\langle\Psi_k|\Psi_k\rangle = |\Psi_0\rangle\end{aligned}\quad (1)$$

where \hat{O}_k^\dagger denotes the deexcitation operator (a Hermitian conjugate of \hat{O}_k). In the context of excitation energy calculations, $|\Psi_0\rangle$ corresponds to the ground electronic state. The commutator of the Hamiltonian and excitation operator \hat{O}_k acting on the ground state yields the excitation energy of k th state

$$[\hat{H}, \hat{O}_k]|\Psi_0\rangle = \omega_{k0}|\Psi_0\rangle = \omega_{k0}\hat{O}_k|\Psi_0\rangle \quad (2)$$

where ω_{k0} is the difference between the k th and the ground-state energies, $\omega_{k0} = E_k - E_0$. Projecting $\hat{O}_k|\Psi_0\rangle$ on the bra side of eq 2, one can show that

$$\begin{aligned} \langle\Psi_0|[\hat{O}_k^\dagger[\hat{H}, \hat{O}_k]]|\Psi_0\rangle &= \frac{\langle\Psi_0|[\hat{O}_k^\dagger, [\hat{H}, \hat{O}_k]]|\Psi_0\rangle}{\langle\Psi_0|\hat{O}_k^\dagger\hat{O}_k|\Psi_0\rangle} \\ &= \frac{\langle\Psi_0|[\hat{O}_k^\dagger, \hat{H}, \hat{O}_k]|\Psi_0\rangle}{\langle\Psi_0|[\hat{O}_k^\dagger, \hat{O}_k]|\Psi_0\rangle} = \omega_{k0} \end{aligned} \quad (3)$$

where the double commutator is defined as $2[\hat{O}_k^\dagger, \hat{H}, \hat{O}_k] = [[\hat{O}_k^\dagger, \hat{H}], \hat{O}_k] + [\hat{O}_k^\dagger, [\hat{H}, \hat{O}_k]]$. All four expressions in eqs 2 and 3 yield identical results in the complete operator basis set or when the killer condition is satisfied⁵⁰

$$\hat{O}_k^\dagger|\Psi_0\rangle = |\Psi_0\rangle\langle\Psi_k|\Psi_0\rangle = 0, \forall k \quad (4)$$

The killer condition means that the ground state $|\Psi_0\rangle$ cannot be deexcited due to the orthogonality condition, $|\Psi_k\rangle \perp |\Psi_0\rangle$.^{36–38}

The killer condition of eq 4 is trivially satisfied when $|\Psi_0\rangle$ is the exact ground state and \hat{O}_k is the exact eigenoperator of \hat{H} . Another way to satisfy the killer condition is to employ a single Slater determinant $|\Phi_0\rangle$ as the reference vacuum state while using \hat{O}_k^\dagger with pure deexcitation operators relative to $|\Phi_0\rangle$. In this case, the operator \hat{O}_k does not have to be complete, e.g.

$$\sum_{\substack{p \in \{i,j,\dots\} \\ q \in \{a,b,\dots\}}} \hat{a}_p^\dagger \hat{a}_q |\Phi_0\rangle = \emptyset \quad (5)$$

where \hat{a}_p^\dagger and \hat{a}_q denote creation and annihilation operators associated with spin-orbitals p and q , and the symbol \emptyset represents an empty state, which is distinct from the Fock vacuum state $|\Phi_0\rangle$. In this paper, we follow the standard convention: i,j,\dots denote spin-orbitals that are occupied in the reference Slater determinant ($|\Phi_0\rangle$), whereas a,b,\dots denote unoccupied (virtual) spin-orbitals. The indices p,q,\dots refer to spin-orbitals that may be either occupied or unoccupied.

To formulate an EOM operator acting on a correlated ground-state wavefunction $|\Psi_0\rangle$ (instead of $|\Phi_0\rangle$), one needs to consider both excitation and deexcitation operators because $|\Psi_0\rangle$ comprises multiple Slater determinants.^{51,52} The general form of the operator \hat{O}_k can be written as a linear combination of particle–hole excitation and deexcitation operators with coefficients $\{X,Y\}$

$$\hat{O}_k = \sum_{\alpha} \sum_{\mu_a} [X_{\mu_a}^k \hat{E}_{\mu_a} - Y_{\mu_a}^k \hat{E}_{\mu_a}^\dagger] \quad (6)$$

where \hat{E} and \hat{E}^\dagger are a set of particle–hole excitation and deexcitation operators, respectively. The subscript α denotes the number of particle–hole pairs to be created in the reference Slater determinant $|\Phi_0\rangle$ and μ_α denotes a set of occupied and virtual spin-orbitals. For example, $\hat{E}_{\mu_1=a,i} = \hat{a}_a^\dagger \hat{a}_i$ creates a one-hole–one-particle (1h1p) determinant from the reference Slater determinant. In practice, the many-electron basis α is truncated

at a particular level to yield a specific model, for example, EOM-CC with singles and doubles (EOM-CCSD)

$$\begin{aligned} \hat{O}_k^{\text{SD}} &= \hat{O}_k^1 + \hat{O}_k^2 \\ \hat{O}_k^1 &= \sum_{ia} [(X_i^a)^k \hat{E}_i^a - (Y_a^i)^k \hat{E}_a^i] \\ \hat{O}_k^2 &= \frac{1}{4} \sum_{ijab} [(X_{ij}^{ab})^k \hat{E}_{ij}^{ab} - (Y_{ab}^{ij})^k \hat{E}_{ab}^{ij}] \end{aligned} \quad (7)$$

A variational minimization of eq 3 with respect to the amplitudes $\{X^k, Y^k\}$ gives rise to the following secular equation

$$\begin{pmatrix} \mathbf{M} & \mathbf{Q} \\ \mathbf{Q}^* & \mathbf{M}^* \end{pmatrix} \begin{pmatrix} \mathbf{X}^k \\ \mathbf{Y}^k \end{pmatrix} = \omega_{k0} \begin{pmatrix} \mathbf{V} & \mathbf{W} \\ -\mathbf{W}^* & -\mathbf{V}^* \end{pmatrix} \begin{pmatrix} \mathbf{X}^k \\ \mathbf{Y}^k \end{pmatrix} \quad (8)$$

where the matrices \mathbf{M} , \mathbf{Q} , \mathbf{V} , and \mathbf{W} are

$$\begin{aligned} \mathbf{M}_{\mu_a \nu_\beta} &= \langle \Psi_0 | [\hat{E}_{\mu_a}^\dagger, \hat{H}, \hat{E}_{\nu_\beta}] | \Psi_0 \rangle \\ \mathbf{V}_{\mu_a \nu_\beta} &= \langle \Psi_0 | [\hat{E}_{\mu_a}^\dagger, \hat{E}_{\nu_\beta}] | \Psi_0 \rangle \\ \mathbf{Q}_{\mu_a \nu_\beta} &= -\langle \Psi_0 | [\hat{E}_{\mu_a}^\dagger, \hat{H}, \hat{E}_{\nu_\beta}^\dagger] | \Psi_0 \rangle \\ \mathbf{W}_{\mu_a \nu_\beta} &= -\langle \Psi_0 | [\hat{E}_{\mu_a}^\dagger, \hat{E}_{\nu_\beta}^\dagger] | \Psi_0 \rangle \end{aligned} \quad (9)$$

In the case of a finite operator basis set, the killer condition does not necessarily hold and the four expressions in eqs 2 and 3 are not equivalent, making the choice of working equations arbitrary.

II.II. Choice of the Ground-State Ansatz: CC versus UCC. The CC theory^{53–56} is designed to compute many-body wavefunctions, typically for the ground state. The standard CC theory represents the many-body wavefunction as an exponential ansatz acting on the reference Slater determinant $|\Phi_0\rangle$

$$\begin{aligned} |\Psi_0\rangle &= |\Psi_{\text{CC}}\rangle = e^{\hat{T}}|\Phi_0\rangle \\ \hat{T} &= \hat{T}_1 + \dots + \hat{T}_N \end{aligned} \quad (10)$$

where \hat{T}_μ represents a μ -fold particle–hole excitation operator (the cluster operator) for the N -electron system (the subscript denotes the number of particle–hole pairs to be created in $|\Phi_0\rangle$). Explicitly,

$$\hat{T}_\mu = \frac{1}{(\mu!)^2} \sum_{\substack{i_1 \cdots i_\mu \\ a_1 \cdots a_\mu}} t_{i_1 \cdots i_\mu}^{a_1 \cdots a_\mu} \hat{a}_{a_1}^\dagger \hat{a}_{i_1} \cdots \hat{a}_{a_\mu}^\dagger \hat{a}_{i_\mu} \quad (11)$$

where $i_1 \cdots i_\mu$ and $a_1 \cdots a_\mu$ are occupied and unoccupied spin-orbital indices in $|\Phi_0\rangle$. In practice, the cluster operator is truncated at a particular level, yielding a specific model such as CCSD, CCSDT, etc. The main advantage of the exponential ansatz over linear parameterization (such as in CI) is that the truncated CC theory is size-extensive.

In the standard CC theory, one solves the equations derived by projecting the Schrödinger equation on the manifold of the excited Slater determinants

$$\begin{aligned} \langle \Phi_0 | \bar{H} | \Phi_0 \rangle &= \mathcal{E}_{\text{CC}} \\ \langle \Phi_{ij\dots}^{ab\dots} | \bar{H} - \mathcal{E}_{\text{CC}} | \Phi_0 \rangle &= 0 \end{aligned} \quad (12)$$

which amounts to satisfying the Schrödinger equation in the subspace of the full Hilbert space. Here, $\tilde{H} \equiv e^{-\hat{T}}\hat{H}e^{\hat{T}}$ is the similarity-transformed Hamiltonian (non-Hermitian) and \mathcal{E}_{CC} is the CC energy (typically, the ground-state energy). Note that the similarity transformation conserves the eigenspectrum of the original Hamiltonian \hat{H} .

Equations 12 are tractable because the infinite Taylor series generated by the exponential ansatz truncate naturally due to the Slater rules (when bra and ket determinants differ by more than double excitations).

The EOM-CC ansatz is built on the ground-state CC theory to describe excited states^{28–31,38,57–60}

$$|\Psi_k\rangle = \hat{R}_k |\Psi_{CC}\rangle = \hat{R}_k e^{\hat{T}} |\Phi_0\rangle \quad (13)$$

where \hat{R}_k denotes the projection operator that generates the k th excited state from the ground-state CC wavefunction. In the single-reference EOM-CC theory, \hat{R}_k consists only of particle–hole excitations manifold with respect to $|\Phi_0\rangle$. Explicitly,

$$\begin{aligned} \hat{R}_k &= R_k^1 + \cdots + R_k^N, \\ \hat{R}_k^\mu &= \frac{1}{(\mu!)^2} \sum_{\substack{i_1 \cdots i_\mu \\ a_1 \cdots a_\mu}} (r_{i_1 \cdots i_\mu}^{a_1 \cdots a_\mu})^k \hat{a}_{a_1}^\dagger \hat{a}_{i_1} \cdots \hat{a}_{a_\mu}^\dagger \hat{a}_{i_\mu} \end{aligned} \quad (14)$$

This choice of the operators means that \hat{R} and \hat{T} commute, leading to the eigenvalue problem for the similarity-transformed Hamiltonian \tilde{H}

$$\tilde{H}\hat{R}_k|\Phi_0\rangle = \mathcal{E}_k \hat{R}_k |\Phi_0\rangle \quad (15)$$

Equation 15 means that the k th excitation energy can be obtained by the commutator of eq 2 acting on $|\Phi_0\rangle$ (and not $|\Psi_0\rangle$)

$$[\tilde{H}, \hat{R}_k]|\Phi_0\rangle = \omega_{k0} \hat{R}_k |\Phi_0\rangle \quad (16)$$

Note that the Hamiltonian for the standard EOM-CC is the similarity-transformed Hamiltonian \tilde{H} . The advantage of the standard, single-reference EOM-CC compared to the general case described in the previous section is that it satisfies the killer condition by construction and that the secular equation of eq 8 becomes an eigenvalue problem

$$\mathbf{M}\mathbf{r}^k = \omega_{k0}\mathbf{r}^k \quad (17)$$

Because \tilde{H} is non-Hermitian, its left eigenstates are not Hermitian conjugates of its right eigenstates and need to be found by solving the left eigenproblem (this additional step is required for computing properties⁶⁰ within the EOM framework).

The quality of EOM-CC results depends on the quality of the ground-state CC wavefunction. Because the CC equations are derived by the projection technique, \mathcal{E}_{CC} is not a variational bound to the exact ground-state energy and can diverge in the strongly correlated regime, when the single Slater determinant is not a good approximation to the exact ground state. Variational formulation of the CC theory solves the divergence problem⁶¹ but is impractical on classical computers because the resulting equations do not truncate. Therefore, it is tempting to consider variational implementation of the CC theory on a quantum device, expecting efficient state preparation, but this is even more challenging because the exponential ansatz of the CC theory is nonunitary.

There exists a unitary version of the coupled-cluster theory, UCC⁶²

$$|\Psi_0\rangle = |\Phi_{UCC}\rangle = e^{\hat{T}-\hat{T}^\dagger} |\Phi_0\rangle = e^{\hat{\sigma}} |\Phi_0\rangle \quad (18)$$

where \hat{T} is the cluster operator of eq 11 and \hat{T}^\dagger is a particle–hole deexcitation operator with respect to $|\Phi_0\rangle$. This ansatz satisfies the condition of unitary operator, $U^\dagger = U^{-1}$, giving rise to $UU^\dagger = 1$

$$(e^{\hat{\sigma}})^\dagger = (e^{\hat{T}-\hat{T}^\dagger})^\dagger = e^{\hat{T}^\dagger-\hat{T}} = e^{-\hat{\sigma}} = (e^{\hat{\sigma}})^{-1} \quad (19)$$

With the unitary ansatz, the energy of UCC (\mathcal{E}_{UCC}) is an upper bound of the exact ground-state energy. The UCC theory results in the Hermitian effective Hamiltonian $e^{-\hat{\sigma}}\hat{H}e^{\hat{\sigma}} \equiv \tilde{H}$ (by using tilde instead of a bar, we distinguish the UCC effective Hamiltonian \tilde{H} from the non-Hermitian \bar{H} of the standard CC theory). The UCC formalism is Hermitian, variational, and size-extensive; however, unlike \bar{H} , the Baker–Campbell–Hausdorff series of \tilde{H} does not terminate naturally making it unfeasible for classical computers. To overcome this problem, several approximations to the UCC ansatz have been developed.^{63–65}

Alternatively, the classically intractable UCC equations can be efficiently implemented on quantum devices¹³ because $\hat{H}e^{\hat{\sigma}}|\Phi_0\rangle$ can be transformed into a polynomial number of terms that act on the initial qubit state through Trotterization^{66,67} and Jordan–Wigner’s transformation,⁶⁸ which can be simulated in polynomial time⁶⁹ on quantum devices.

Following earlier work,^{32,40} we use UCC as the ground-state ansatz on top of which we build the EOM ansatz, giving rise to EOM-UCC. Specifically, we derive and utilize the effective Hamiltonian presented in ref 32 to develop the excited-state algorithms for quantum solvers.

The unitary operator $e^{\hat{\sigma}}$ and the projection operator $\hat{O}_k(\{\hat{E}_\mu\}$ or $\{\hat{E}_\mu\} \cup \{\hat{E}_\mu^\dagger\}$) do not commute. Therefore, EOM-UCC does not satisfy the killer condition with the finite operator basis set. The immediate negative consequence of violating the killer condition is that the equality condition of eq 3 does not hold. Mukherjee and co-workers proposed the so-called self-consistent manifold $\{\hat{S}_\mu\} \cup \{\hat{S}_\mu^\dagger\}$ in the UCC-based self-consistent polarization propagator theory, which is a unitary transformation of operator manifold of \hat{O}_k ^{37,39}

$$\hat{S}_\mu = e^{\hat{\sigma}} \hat{E}_\mu e^{-\hat{\sigma}} \quad (20)$$

where \hat{E}_μ are the original particle–hole excitation operators that span the space of \hat{O}_k . The UCC amplitudes entering $e^{\hat{\sigma}}$ are known from the ground-state UCC calculation. Adopting $\{\hat{S}_\mu\} \cup \{\hat{S}_\mu^\dagger\}$ instead of $\{\hat{E}_\mu\} \cup \{\hat{E}_\mu^\dagger\}$ for eq 9, the matrix elements M of eq 9 can be written as

$$\begin{aligned} M_{\mu_\alpha \nu_\beta} &= \langle \Psi_0 | [\hat{S}_{\mu_\alpha}^\dagger, \hat{H}, \hat{S}_{\nu_\beta}] | \Psi_0 \rangle \\ &= \langle \Psi_0 | [e^{\hat{\sigma}} \hat{E}_{\mu_\alpha}^\dagger e^{-\hat{\sigma}}, \hat{H}, e^{\hat{\sigma}} \hat{E}_{\nu_\beta} e^{-\hat{\sigma}}] | \Psi_0 \rangle \\ &= \langle \Phi_0 | e^{-\hat{\sigma}} [e^{\hat{\sigma}} \hat{E}_{\mu_\alpha}^\dagger e^{-\hat{\sigma}}, \hat{H}, e^{\hat{\sigma}} \hat{E}_{\nu_\beta} e^{-\hat{\sigma}}] e^{\hat{\sigma}} | \Phi_0 \rangle \\ &= \langle \Phi_0 | \hat{E}_{\mu_\alpha}^\dagger e^{-\hat{\sigma}} \hat{H} e^{\hat{\sigma}} \hat{E}_{\nu_\beta} | \Phi_0 \rangle \\ &= \langle \Phi_0 | \hat{E}_{\mu_\alpha}^\dagger \tilde{H} \hat{E}_{\nu_\beta} | \Phi_0 \rangle \end{aligned} \quad (21)$$

The matrix elements Q and W of eq 9 become $\mathbf{0}$, and V becomes \mathbf{I} , giving rise to

$$\begin{pmatrix} \mathbf{M} & \mathbf{0} \\ \mathbf{0} & \mathbf{M}^* \end{pmatrix} \begin{pmatrix} \mathbf{X}^k \\ \mathbf{Y}^k \end{pmatrix} = \omega_{k0} \begin{pmatrix} \mathbf{I} & \mathbf{0} \\ \mathbf{0} & -\mathbf{I} \end{pmatrix} \begin{pmatrix} \mathbf{X}^k \\ \mathbf{Y}^k \end{pmatrix} \quad (22)$$

With self-consistent manifold operators, EOM-UCC satisfies the killer condition and the equations can be cast in the form of an eigenvalue equation, such as eq 17 of the EOM-CC method but with the UCC effective Hamiltonian \tilde{H} .

II.III. Solving q-sc-EOM-UCCSD on Quantum Computers Using a Davidson-Like Procedure. Similar to the classical electronic structure calculations, the quantum self-consistent equation-of-motion (q-sc-EOM) protocol computes the ground state before solving the EOM problem by using the variational quantum eigensolver (VQE)^{3,13,14,16,70,71} with the choice of an appropriate ansatz, such as unitary coupled-cluster (UCC)³⁵ and Hardware-efficient ansatz.¹⁶ As discussed in the previous section, we use the UCC ansatz with single and double substitutions (q-sc-EOM-UCCSD)

$$\hat{T} = \hat{T}_1 + \hat{T}_2 = \sum_{ia} \theta_i^a a_a^\dagger a_i + \frac{1}{4} \sum_{ijab} \theta_{ij}^{ab} a_a^\dagger a_b a_b^\dagger a_j \quad (23)$$

where $\{\theta\}$ represents the set of variational parameters (same as the cluster amplitudes $\{t\}$ in classical simulations). The ground-state wavefunction in eqs 2–9 is replaced with the VQE-UCCSD ground-state wavefunction. The ground-state VQE minimizes the expectation value of the Hamiltonian with respect to the variational parameters $\{\theta_i^a, \theta_{ij}^{ab}\}$

$$\mathcal{E}_0(\theta_i^a, \theta_{ij}^{ab}) = \min_{\theta_i^a, \theta_{ij}^{ab}} \langle \Psi_{\text{VQE}}(\theta_i^a, \theta_{ij}^{ab}) | \hat{H} | \Psi_{\text{VQE}}(\theta_i^a, \theta_{ij}^{ab}) \rangle \quad (24)$$

In order to compute electronic excitation energies on quantum devices, the q-sc-EOM ansatz is applied to the ground-state VQE wavefunction (ground-state VQE circuit with optimized parameters). q-sc-EOM measures the matrix elements of \tilde{H} of eq 21 on a quantum device and then solves the eigenvalue problem of eq 22 on a classical computer. Equations 21 and 22, which are the working equation of q-sc-EOM, are the same as in the standard EOM-CC method except for the form of the effective Hamiltonian. In the standard EOM-CC calculation, we iteratively determine only a few eigenvalues using the Davidson algorithm^{41–43} instead of explicit diagonalization of the entire matrix M . Here, we present the implementation of this idea within the q-sc-EOM method (we focus on the standard Davidson algorithm for low-lying states, but it can be extended to compute interior states or states of a particular character⁴⁴).

To compute J excited states, a minimum of J guess vectors are required, but in practice $L(>J)$ guess vectors are often used to expand the span of the guess vector space. q-sc-EOM-UCC/Davidson starts with generating a set of appropriate L orthonormal guess vectors, $\{|b_i\rangle\}_{i=1}^L$. Then, we measure the matrix elements of \tilde{H} in the given guess vector space and build the subspace Hamiltonian using a quantum device

$$\tilde{H}_{ij}^{\text{sub}} = \langle b_i | \tilde{H} | b_j \rangle = \langle \Phi_0 | \hat{U}_i^\dagger \tilde{H} \hat{U}_j | \Phi_0 \rangle, \quad 1 \leq i, j \leq L \quad (25)$$

where \hat{U}_μ denotes unitary operators that transform $|\Phi_0\rangle$ into the qubit state $|b_\mu\rangle$. Using a classical computer, we then diagonalize the subspace Hamiltonian and obtain L approximate eigenvectors and the corresponding eigenvalues

$$\tilde{H}^{\text{sub}} |c^k\rangle = \lambda^k |c^k\rangle, \quad k = 1, \dots, L \quad (26)$$

where λ^k and $|c^k\rangle$ denote approximate k th eigenvalue and eigenvector in the given guess vector space, respectively. We then select J eigenvectors and the corresponding eigenvalues from the obtained set of L vectors using appropriate criteria—for example, in the most basic version in which the algorithm is looking for J lowest states, the lowest-energy solutions are selected (different vector selection schemes can be implemented depending on the desired group of transitions⁴⁴). These vectors approximate the solutions and are used to evaluate the convergence. As in the classical Davidson method, the computed J eigenvectors are the linear combination of the guess vectors

$$|c^k\rangle = \sum_{i=1}^L c_i^k |b_i\rangle \quad (27)$$

where c_i^k denotes the expansion coefficient of i th guess vector for the approximate k th eigenvector. At each iteration, the algorithm computes the deviation of the approximate eigenvectors, $|c^k\rangle$, from the true eigenvectors by computing the residual vectors

$$|r^k\rangle = (\tilde{H} - \lambda^k) |c^k\rangle = \sum_{i=1}^L c_i^k (\tilde{H} - \lambda^k) |b_i\rangle, \quad k = 1, \dots, J \quad (28)$$

As per eq 28, the residual vectors are zero for the true eigenvectors. The convergence is assessed by the norm of residual vectors, which also can be measured on quantum devices. The residual vectors $|r^k\rangle$ are linear combinations of excited Slater determinants. Thus, the evaluation of the norms of residual vectors is equivalent to probing the composition of Slater determinants and residual vectors

$$\|r^k\| = \sqrt{\sum_{\mu=1}^N |\langle \Phi_\mu | r^k \rangle|^2} \quad (29)$$

Note that $\{c_i^k\}_{i=1}^L$, $\{\lambda^k\}_{k=1}^J$, and $\{|b_i\rangle\}_{i=1}^L$ of eq 28 are already known from the previous steps. Therefore, the q-sc-EOM-UCC/Davidson only measures the overlap between Slater determinants and σ -vectors $\langle \Phi_\mu | \sigma_i \rangle$. The final step of the q-sc-EOM-UCC/Davidson algorithm is the orthonormalization of the residual vectors to the current set of guess vectors and expansion of the vector space with the (orthonormalized) residuals. This can be done by the Gram–Schmidt procedure⁷² on classical computers

$$|b_k\rangle = |r^k\rangle - \sum_{i=1}^{k-1} \langle r^k | b_i \rangle |b_i\rangle \quad (30)$$

$$|b_k^{\text{corr}}\rangle = \frac{|b_k\rangle}{\langle b_k | b_k \rangle} \quad (31)$$

where $|b_k^{\text{corr}}\rangle$ denotes the correction vector for the k th state. Finally, the correction vectors are added to the guess vector space. The algorithm repeats steps 25–31 until convergence is reached. The guess vector space is expanded at each iteration by including the maximum of J correction vectors.

II.IV. Gray Code Decomposition. The ground state is the lowest-energy eigenstate. The existing state preparation schemes, such as UCCSD³⁵ and hardware-efficient ansatz,¹⁶ are designed to effectively search the Hilbert space of a quantum system. They are commonly used to provide trial wavefunctions

in the VQE method for searching the ground state. Excited-state preparation schemes require additional features compared to those of the ground state. For example, the excited-state ansatz should be capable of producing particular electronic configurations out of the entire Hilbert space (e.g., singlet-coupled HOMO–LUMO excitation). In addition, the ansatz should be able to easily adjust the components of a desired quantum state. Consider, for instance, the H₂/6-31G example for which the number of all possible electronic configurations is $\binom{8}{2}$. To compute the S₁ state (at 1 Å bondlength), we need to prepare the superposition of two singly excited configurations (excitation from σ to σ^* with respect to the reference vacuum state |11000000⟩) with the equal weights as an initial guess vector |b₁⟩. In the qubit representation, the initial guess vector is

$$|b_1\rangle = \frac{1}{\sqrt{2}}(|01100000\rangle - |10010000\rangle) \quad (32)$$

where |0⟩ and |1⟩ represent unoccupied and occupied spin-orbitals, respectively. Here, we map the spin-orbitals onto the qubits in the left-to-right order, such that the lowest-energy orbitals are at the left most, to be consistent with our implementation using the OpenFermion platform.^{73,74} α spin-orbitals (|↑⟩) are mapped onto the even-numbered qubits (0th, 2nd,...) and β spin-orbitals (|↓⟩) are mapped onto the odd-numbered qubits (1st, 3rd,...). Figure 1 shows the electronic

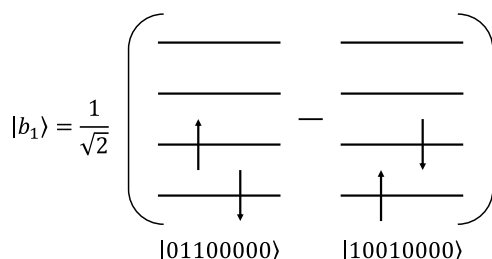


Figure 1. Electronic configuration of the initial guess vector of eq 32.

configuration of |b₁⟩ of eq 32. The first iteration of the Davidson algorithm results in the correction vector

$$\begin{aligned} |b_2\rangle = & 0.6506(|00000110\rangle - |00000110\rangle) + 0.2369 \\ & (|00011000\rangle - |00100100\rangle) + 0.1434(|01000010\rangle \\ & - |10000001\rangle) \end{aligned} \quad (33)$$

As per eqs 32 and 33, one needs to design unitary operations that transform an arbitrary qubit state $\otimes_{i=0}^{n-1}|0\rangle$ into a particular

superposition state, i.e., the quantum state consisting of particular excited Slater determinants. In addition, the relative phases between the determinants should be easily adjustable within the reduced Hilbert space.

In order to demonstrate the general state preparation algorithm for the q-sc-EOM-UCC/Davidson method, we consider a simple example—two particles in four spin-orbitals—for which the subspace is spanned by six electronic configurations, { |1100⟩, |0110⟩, |1001⟩, |0101⟩, |1010⟩, |0011⟩ }. Considering excitations that conserve spin projection ($\Delta m_s = 0$), one needs unitary operators that transform the initial reference qubit state (typically, the Hartree–Fock determinant, |1100⟩) into the superposition of four particular electronic configurations with a set of controllable parameters

$$\begin{aligned} U(\theta_3)U(\theta_2)U(\theta_1)|1100\rangle = & \cos \frac{\theta_1}{2} \cos \frac{\theta_2}{2} \cos \frac{\theta_3}{2} |1100\rangle \\ & + \sin \frac{\theta_1}{2} |0110\rangle + \cos \frac{\theta_1}{2} \sin \frac{\theta_2}{2} |1001\rangle \\ & + \cos \frac{\theta_1}{2} \cos \frac{\theta_2}{2} \sin \frac{\theta_3}{2} |0011\rangle \end{aligned} \quad (34)$$

Equation 34 implies that the successive operations of $U(\theta_1)$, $U(\theta_2)$, and $U(\theta_3)$ on the reference state generate a particular target determinant at each operation. In addition, adjustable parameters are introduced to both reference |1100⟩ ($\cos \frac{\theta_1}{2}$) and

target configurations ($\sin \frac{\theta_i}{2}$). This parameterization scheme ensures normalization of the resulting qubit state and facilitates the incorporation of spin symmetries. For example, a triplet excited state can be generated only with $U(\theta_1)$ and $U(\theta_2)$ with the specific values of θ_1 and θ_2

$$U(\theta_2 = \pi)U(\theta_1 = \frac{\pi}{2})|1100\rangle = \frac{1}{\sqrt{2}}(|1001\rangle + |0110\rangle) \quad (35)$$

A singlet excited state with only singly excited determinants can be generated in a similar fashion

$$U(\theta_2 = \pi)U(\theta_1 = -\frac{\pi}{2})|1100\rangle = \frac{1}{\sqrt{2}}(|1001\rangle - |0110\rangle) \quad (36)$$

To construct a quantum circuit for this task, we utilize the Gray code decomposition,^{45,46} which allows one to connect two arbitrary qubit states by sequential bit flips. An example of the Gray code quantum circuit that generates the qubit state of eq 34 is shown in Figure 2. The process of populating a desired

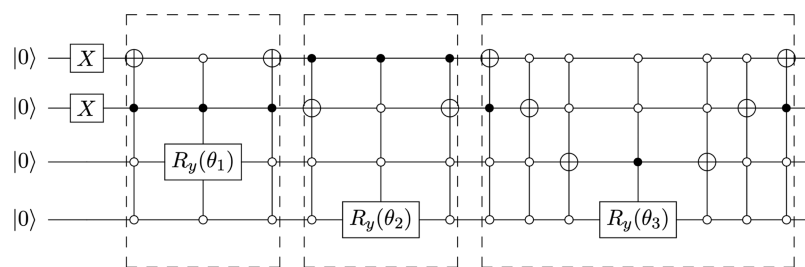


Figure 2. 4-Qubit quantum circuit that generates a superposition state of eq 34 using the Gray code decomposition. Initially applied Pauli-X (NOT) gates transform the vacuum state into the two-particle subspace. Each dashed box represents unitary operation $U(\theta)$ shown in eq 34. The first two blocks induce single excitation and the last performs double excitation with respect to the reference vacuum |1100⟩ to generate |0110⟩, |1001⟩, and |0011⟩, respectively. Each $R_y(\theta)$ gives rise to the $\frac{\theta}{2}$ amplitude. For the triplet subspace of eq 35, the third block is not needed.

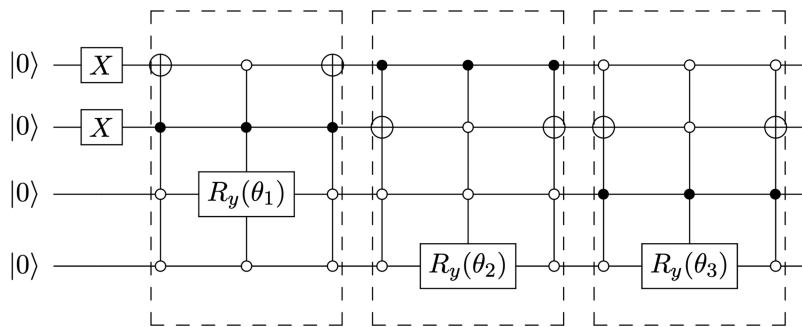


Figure 3. 4-Qubit quantum circuit that generates a superposition state of eq 37 using the Gray code decomposition. The first two blocks induce single excitations with respect to the reference state, $|1100\rangle$. The last block performs single excitation with respect to the configuration $|0110\rangle$ to generate $|0011\rangle$.

quantum state starts with the transformation of the initial qubit state $\otimes_{i=0}^{n-1}|0\rangle$ into N -particle subspace, where n and N correspond to the number of qubits and particles in the system of interest. Next, one designs unitary operators using the Gray code decomposition as shown in the example quantum circuit of Figure 2. Each box in Figure 2 denotes a unitary operation $U(\theta_i)$ constructed using Gray code decomposition to populate the target state from the reference qubit state. Similar to the classical electronic structure procedure, the quantum circuit of $U(\theta_i)$ performs the action of creation and annihilation operators on the reference state introducing an expansion coefficient. Here, we generalize the structure of $U(\theta_i)$ with $2(2M - 1)$ number of multiqubit controlled-NOT gates and one multiqubit controlled- $R_y(\theta_i)$ gate. In total, $4M - 1$ multiqubit controlled gates are applied, where M represents the level of excitations such as singles, doubles, etc. The first $2M - 1$ multiqubit controlled-NOT gates create M holes and $M - 1$ particles with respect to the reference qubit state. The subsequent multiqubit controlled- $R_y(\theta_i)$ creates an additional particle to the state (completion of MhMp excitation) as well as introduces the parameters to the reference $(\cos \frac{\theta}{2})$ and target excited determinant $(\sin \frac{\theta}{2})$. The Gray code for the single unitary operation is completed by the same $2M - 1$ multiqubit controlled-NOT gates, but in the reversed order. It should be mentioned that the target electronic configurations do not have to be populated from the fixed reference state. For example, the doubly excited determinant of eq 34 can be created from one of the singly excited determinants giving rise to different parameterizations

$$\begin{aligned} & U'(\theta_3)U(\theta_2)U(\theta_1)|1100\rangle \\ &= \cos \frac{\theta_1}{2} \cos \frac{\theta_2}{2} |1100\rangle + \sin \frac{\theta_1}{2} \cos \frac{\theta_3}{2} |0110\rangle \\ &+ \cos \frac{\theta_1}{2} \sin \frac{\theta_2}{2} |1001\rangle + \sin \frac{\theta_1}{2} \sin \frac{\theta_3}{2} |0011\rangle \end{aligned} \quad (37)$$

where $U(\theta_1)$ and $U(\theta_2)$ are the same operators demonstrated in eq 34 and the doubly excited configuration $|0011\rangle$ is generated by applying the single excitation operator $U'(\theta_3)$ to the configuration $|0110\rangle$. The quantum circuit that generates the quantum state of eq 37 is shown in Figure 3. An arbitrary quantum superposition state can be generated using only single excitation operators using the Gray code scheme resulting in a smaller number of multiqubit controlled-NOT gates than the aforementioned scheme. We decompose the quantum circuits of Figures 2 and 3 into the elementary single and two-qubit gates using the IBM Qiskit software.⁷⁵ The gate decompositions result in 316 generic single-qubit rotation gates and 200 CNOT gates

for the quantum circuit of Figure 2. Alternatively, the quantum circuit of Figure 3 requires 224 generic single-qubit rotation and 144 CNOT gates. As can be seen from the numerical gate counts, the Gray code scheme with only single excitations yields a compact quantum circuit. In this paper, however, we employ the fixed reference scheme to facilitate the generalization of circuit constructions.

The q-sc-EOM-UCC/Davidson protocol needs quantum devices to measure the matrix elements of \tilde{H} and the norm of residual vectors, as per eqs 25 and 29. This contains a large number of off-diagonal element measurements, $\langle b_i|\tilde{H}|b_j\rangle_{i \neq j}$ and $\langle \Phi_\mu|\tilde{H}|b_i\rangle$, which usually require an ancilla qubit, in addition to the diagonal elements,^{76–79} $\langle b_i|\tilde{H}|b_i\rangle$. Note that $\langle b_i|\tilde{H}|b_j\rangle = \langle \Phi_0| \hat{U}_i^\dagger \hat{H} \hat{U}_j |\Phi_0\rangle$ and $\langle \Phi_\mu|\tilde{H}|b_i\rangle = \langle \Phi_0| E_\mu^\dagger \tilde{H} E_\mu |\Phi_0\rangle$, where \hat{U}_i and E_μ are the unitary operators that transform the reference qubit state $|\Phi_0\rangle$ into the guess vector (linear combination of excited Slater determinants) and excited configuration, respectively. Using the Gray code state preparation scheme, we can measure the off-diagonal elements without adding an ancilla qubit^{20,40} because we can directly construct unitary operators that connect $|b_i\rangle$ and $|b_j\rangle$ (or $|\Phi_\mu\rangle$) states

$$\begin{aligned} \hat{V}_{ij}|\Phi_0\rangle &= \frac{1}{\sqrt{2}}(|b_i\rangle + |b_j\rangle) \\ \langle \Phi_0| \hat{V}_{ij}^\dagger \tilde{H} \hat{V}_{ij} |\Phi_0\rangle_{i \neq j} &= \frac{1}{2}\langle b_i|\tilde{H}|b_i\rangle + \frac{1}{2}\langle b_j|\tilde{H}|b_j\rangle + \langle b_i|\tilde{H}|b_j\rangle \end{aligned} \quad (38)$$

where \hat{V}_{ij} denotes unitary operators that connect arbitrary $|b_i\rangle$ and $|b_j\rangle$. We distinguish it from \hat{U}_i where unitary operators generate arbitrary $|b_i\rangle$. Hence, we can extract the off-diagonal element $\langle b_i|\tilde{H}|b_j\rangle_{i \neq j}$ by subtracting eq 38 by diagonal elements of \tilde{H}

$$\begin{aligned} \langle b_i|\tilde{H}|b_j\rangle_{i \neq j} &= \langle \Phi_0| \hat{V}_{ij}^\dagger \tilde{H} \hat{V}_{ij} |\Phi_0\rangle - 2\langle \Phi_0| \hat{U}_i^\dagger \tilde{H} \hat{U}_i |\Phi_0\rangle \\ &- 2\langle \Phi_0| \hat{U}_j^\dagger \tilde{H} \hat{U}_j |\Phi_0\rangle \end{aligned} \quad (39)$$

The three terms on the right-hand side of eq 39 can be measured on quantum devices without adding ancilla qubits. The sketch of the quantum circuit for measuring matrix elements of \tilde{H} and the flowchart of the q-sc-EOM-UCC/Davidson algorithm are shown in Figures 4 and 5.

II.V. Variational Implementation of q-sc-EOM-UCC/Davidson. The q-sc-EOM-UCC/Davidson algorithm utilizes classical computers to diagonalize \tilde{H}^{sub} and orthogonalized residual vectors by the Gram–Schmidt procedure. The variational implementation of q-sc-EOM-UCC/Davidson re-

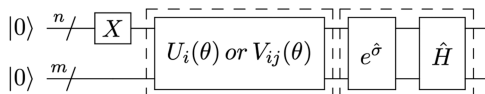


Figure 4. Sketch of quantum circuit for measuring the matrix element of \tilde{H} . n and m denote the number of occupied and virtual orbitals, i.e., $n + m$ corresponds to the total number of required qubits. Initially applied Pauli-X (NOT) gates transform the vacuum state into the reference vacuum state, $|\Phi_0\rangle$ (n -particle subspace). The first dashed box ($U_i(\theta)$ or $V_{ij}(\theta)$) represents unitary operators that transform $|\Phi_0\rangle$ into $|b_i\rangle$ or $|b_i\rangle + |b_j\rangle$. The subsequent operators represent ground-state UCCSD ansatz and molecular Hamiltonian giving rise to the UCCSD Hamiltonian, \tilde{H} .

duces the requirements for both quantum and classical resources. This is achieved by replacing the Gram–Schmidt step and the matrix element measurements step with the expectation-value calculation of \tilde{H} . At each iteration, the Davidson algorithm grows the guess vector space and subsequently diagonalizes \tilde{H} in the updated space. As per eqs 26 and 27, the resulting solution is a linear combination of the guess vectors within the current vector space. Note that the individual guess vectors are a linear combination of excited Slater determinants that are expected to contribute to the current target states, i.e., the solution of an arbitrary k th state in eq 27 can be rewritten as

$$\begin{aligned} |c^k\rangle &= \sum_{i=1}^L c_i^k |b_i\rangle = \sum_{i=1}^L \sum_{\mu} c_i^k \beta_{\mu}^i |\Phi_{\mu}^i\rangle = \sum_{\mu} \sum_{i=1}^L c_i^k \beta_{\mu}^i |\Phi_{\mu}^i\rangle \\ &= \sum_{\mu} \gamma_{\mu}^k |\Phi_{\mu}\rangle \end{aligned} \quad (40)$$

where μ represents a set of indices for occupied and virtual spin-orbitals. The state vector $|\Phi_{\mu}^i\rangle$ with the corresponding coefficient β_{μ}^i denotes the excited Slater determinant (the building block of the guess vector $|b_i\rangle$). This implies that the problem is to find the optimal linear combination of excited Slater determinants, which yields the minimum expectation value of the Hamiltonian.

Considering the Davidson method,^{41–43} the particular set of $\{|\Phi_{\mu}\rangle\}$ can be obtained by examining the residual vectors. Hence, one needs to construct the quantum circuit that generates an arbitrary vector subspace where $\{|\Phi_{\mu}\rangle\}$ spans, and introduce the corresponding $\{\gamma_{\mu}^k\}$ as variational parameters to find a k th state. Since the number of state vectors (= the number of variational parameters) that construct the vector subspace is considerably smaller than that of the entire Hilbert space, the variational approach with the Davidson formalism helps to circumvent the barren plateaus phenomenon.⁸⁰

In practical applications, we need to preserve the spin symmetry and ensure the orthonormality between the eigenstates of the Hamiltonian in the course of the minimization process. To achieve this, we generalize the spin-restricted form of the Gray code circuit with minor modifications of the scheme introduced in the previous section. To illustrate this, let us examine the H₂/STO-3G system, which corresponds to eq 34, and try to find the S₁ state variationally. The Gray code scheme for the nonvariational approach in the previous section creates the desired quantum superposition by connecting the fixed reference state with the target excited Slater determinant at a time. In this way, one introduces parameters to both the reference and target configurations at each operation. There is no direct connection between the excited configurations, which have to be spin-adapted, e.g., between $|0110\rangle$ and $|1001\rangle$ of eq 34. As a result, the variational process with this circuit construction never produces an S₁ state as the solution because the T₁ state is always lower than S₁ in H₂/STO-3G. Furthermore, the variational solution is not necessarily spin pure. Here, we generalize the spin-restricted scheme by “direct connection” between configurations, which have to be spin-adapted. “Direct connection” implies, for example, the configuration $|1001\rangle$ of eq 34 is populated by $|0110\rangle$ not by the fixed reference $|1100\rangle$ (or vice versa)

qEOM-UCC/Davidson

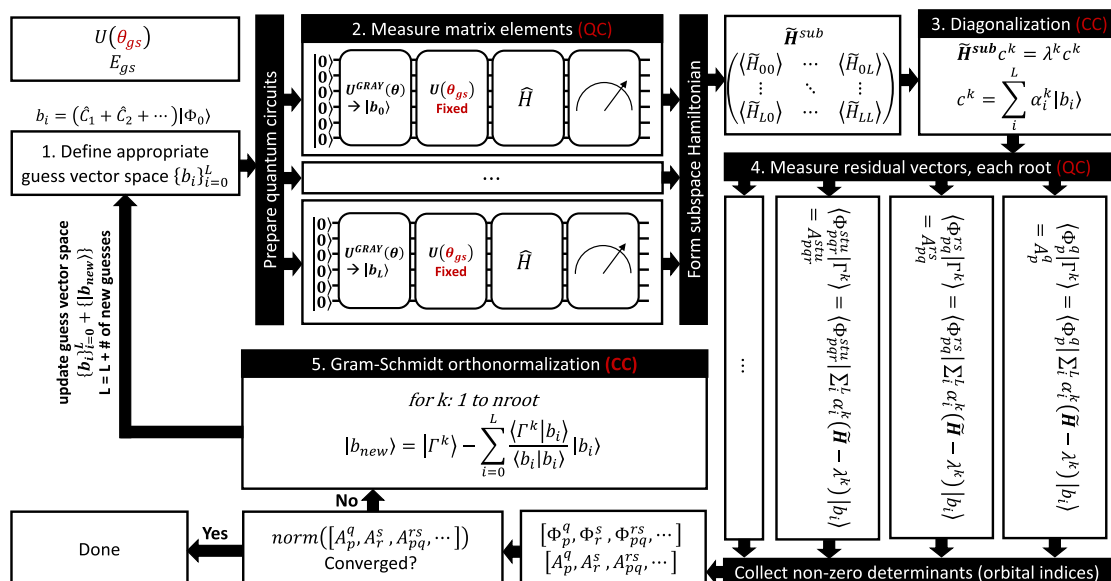


Figure 5. Sketch of the q-sc-EOM-UCC/Davidson algorithm. “QC” and “CC” refer to the quantum computer and classical computer, respectively. $\{|\Phi_p^{r...}\rangle\}$ and $\{A_p^{r...}\}$ represent excited Slater determinants and their degrees of overlap with residual vector $\{|\Gamma^k\rangle\}$. Orbital indices p,q,r,s,\dots refer to spatial orbitals.

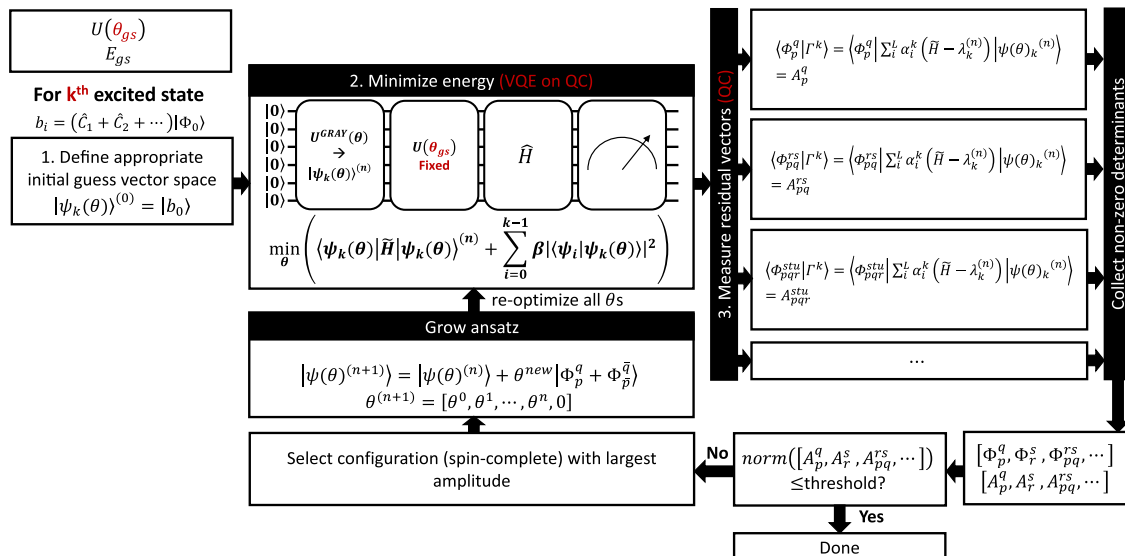
qEOM-UCC/Davidson/Variational

Figure 6. Sketch of the variational extension of the q-sc-EOM-UCC/Davidson algorithm in which matrix element measurement, diagonalization, and Gram–Schmidt procedures are replaced by expectation-value calculations on quantum devices. To guarantee orthogonal eigenstates, the VDQ algorithm is implemented. Orbital indices p,q,r,s,\dots refer to spatial orbitals; the overbar denotes β spin and orbital indices without overbars denote α spin.

$$\begin{aligned} & U(\theta_3)U(\theta_2)U(\theta_1)|1100\rangle \\ &= \cos \frac{\theta_1}{2} \cos \frac{\theta_3}{2} |1100\rangle \\ &+ \sin \frac{\theta_1}{2} \left(\cos \frac{\theta_2}{2} |0110\rangle + \sin \frac{\theta_2}{2} |1001\rangle \right) \\ &+ \cos \frac{\theta_1}{2} \sin \frac{\theta_3}{2} |0011\rangle \end{aligned} \quad (41)$$

where $U(\theta_1)$ and $U(\theta_3)$ connect $|1100\rangle$ with $|0110\rangle$ and $|0011\rangle$. In contrast, $U(\theta_2)$ is applied for $|0110\rangle$ (not $|1100\rangle$) to create $|1001\rangle$. By setting $\theta_2 = -\frac{\pi}{2}$ and $\theta_3 = \pi$, one can create variational ansatz that spans only the excited singlet subspace

$$|\Psi(\theta_1)\rangle = \sin \frac{\theta_1}{2} \left(\frac{|0110\rangle - |1001\rangle}{\sqrt{2}} \right) + \cos \frac{\theta_1}{2} |0011\rangle \quad (42)$$

As can be seen from eq 42, the parameters for the spin-adapted configurations are not treated variationally. Depending upon the desired spin state, the algorithm employs $\frac{\pi}{2}$ for the positive and $-\frac{\pi}{2}$ for the negative combinations.

To ensure the orthonormality of the eigenstates of \tilde{H} , we use the VQD method,¹⁹ the extension of VQE to compute the k th excited state by minimizing the following cost function

$$\begin{aligned} F(\{\theta_k\}) &= \langle \Psi(\{\theta_k\}) | \tilde{H} | \Psi(\{\theta_k\}) \rangle \\ &+ \sum_{i=0}^{k-1} W_i |\langle \Psi(\{\theta_k\}) | \Psi(\{\theta_i\}) \rangle|^2 \end{aligned} \quad (43)$$

where $\{\theta_k\}$ represents the set of variational parameters optimized to obtain the minimum E_k . $\{\theta_i\}$ is the set of variational parameters that is already determined for the state $|\Psi_i\rangle_{i=0,\dots,k-1}$. $\{W_i\}$ is the set of sufficiently large real-valued coefficients. Hence, the minimization of $F(\{\theta_k\})$ means to minimize the E_k with the constraint that $|\Psi(\{\theta_k\})$ is orthogonal

to the states $|\Psi_0\rangle, \dots, |\Psi_{k-1}\rangle$. In the q-sc-EOM-UCC/Davidson/Variational algorithm, we include a single set of spin-adapted determinants into the ansatz at a time, similar to the ADAPT algorithm for the ground state.⁸¹ The determinants are selected based on the overlaps between the residual vector and the excited Slater determinants, as per eq 29. The algorithm repeats until the norm of the residual vector satisfies the set convergence criteria. Figure 6 shows the flowchart of the q-sc-EOM-UCC/Davidson/Variational algorithm.

II.VI. Computational Details. Following ref 32, we use the acronym q-sc-EOM-UCC/Davidson(/Variational) to distinguish it from standard EOM-CC. All simulations were performed using the OpenFermion–Q-Chem interface.⁷⁴ The source code and data used in this work are available on github.⁸² One-electron and two-electron integrals are computed using the Q-Chem⁸³ electronic structure package. The Jordan–Wigner transformation⁶⁸ is carried out to convert the fermionic operators into qubit representation using the OpenFermion package.⁷³ q-sc-EOM-UCC/Davidson(/Variational) begins after ground-state VQE. The ground-state energy and wavefunction are obtained using the ADAPT-VQE method with the generalized singles and doubles (GSD) operator pool.^{81,84} Wavefunction optimization is carried out via the Broyden–Fletcher–Goldfarb–Shannon (BFGS) implemented in Scipy package⁸⁵ with the gradient convergence criterion of 10^{-3} . Quantum circuits for the excited-state calculations are constructed using Cirq python library.⁸⁶ The convergence threshold (the norm of the residual vectors) was 10^{-3} . The pool of the excited Slater determinants is restricted to the singles and doubles. For the variational approach, $\{W_i\}$ of eq 43 is set to 10.0 E_h for all excited states. Likewise the ground-state calculation, the BFGS optimizer is employed to minimize the cost function of eq 43. To validate the performance and accuracy of the suggested algorithms, a classical state-vector type of simulator is used for all ground and excited-state calculations where the exact unitary operations (noise-free) are applied to the wavefunction.

The q-sc-EOM-UCCSD/Davidson calculation begins by defining appropriate initial guess vectors. Similar to the standard EOM-CC, we define the initial guess vectors based on the diagonal elements of the UCCSD Hamiltonian \tilde{H} . Considering $H_2/6-31G$ at 1.0 Å bondlength, σ to σ^* transitions (HOMO to LUMO) give rise to the lowest-energy difference. Two configurations are degenerate in energy, such that the equal superposition of two determinants is chosen for the first excitation energy computation. The relative phase between two configurations is appropriately adjusted depending on the spin symmetry. For the S_2 state, the next lowest diagonal elements are considered, namely, double excitation involving $(\sigma_\alpha\sigma_\beta)$ to $(\sigma_\alpha^*\sigma_\beta^*)$. All computations follow the same procedure of generating the initial guesses except for the singlet calculations of $H_4/STO-3G$ system and some triplet calculations of $H_2O/STO-3G$ system. The initial guess vectors for the case of exceptions are collected in Table 1.

Table 1. Initial Guess Vectors for Exceptions^a

molecule	$\langle S^2 \rangle$	r (Å)	target state	initial guess vector
$H_4/STO-3G$	0.0	1.8–2.4	S_1	$ \Phi_{23}^{45}\rangle$
			S_2	$\frac{1}{\sqrt{2}}(\Phi_3^5\rangle - \Phi_2^4\rangle)$
			S_3	$\frac{1}{\sqrt{2}}(\Phi_3^7\rangle - \Phi_2^6\rangle)$
	0.9	T ₁		$\frac{1}{\sqrt{2}}(\Phi_6^8\rangle + \Phi_7^9\rangle)$
			T ₂	$\frac{1}{\sqrt{2}}(\Phi_4^8\rangle + \Phi_5^9\rangle)$
	2.0	T ₁		$\frac{1}{\sqrt{2}}(\Phi_4^8\rangle + \Phi_5^9\rangle)$
$H_2O/STO-3G$	1.5–1.6	T ₂		$\frac{1}{\sqrt{2}}(\Phi_6^8\rangle + \Phi_7^9\rangle)$

^aQubit index starts from 0.

III. RESULTS AND DISCUSSION

III.I. Resource Requirements. We begin by discussing the computational complexities of the q-sc-EOM algorithm. The q-sc-EOM method utilizes both classical and quantum devices to compute molecular excitation energies. The number of matrix elements that need to be measured on quantum computers and the dimension of the matrix that needs to be diagonalized on classical computers depend on the level of correlation treatment and the one-electron basis set used. When restricting the excitation levels to singles and doubles, the quantum computer needs to measure approximately $O(n_{occ}^4 n_{vir}^4)$ matrix elements, where n_{occ} and n_{vir} represent the number of occupied and virtual spin-orbitals, respectively. Consequently, the overall scaling of quantum shots required to measure the matrix elements of M is approximately $O(\eta^4 n_{occ}^4 n_{vir}^4)$, where η denotes the total number of spin-orbitals (qubits), $n_{occ} + n_{vir}$. Additionally, the classical computer needs to diagonalize the matrix M , which scales as $O(n_{occ}^6 n_{vir}^6)$, because the dimension of M scales as $O(n_{occ}^2 n_{vir}^2)$. While utilizing the sparsity and symmetries of the Hamiltonian can significantly reduce the overall shot scaling and the dimension of matrix M , the scaling quickly becomes intractable as the system size increases.

The implementation of the Davidson method affords significant reductions in both quantum and classical complexities. Specifically, there are two distinct quantum measurement steps involved: the measurement of the matrix elements of M and the measurement of the residual vectors. By restricting the excitation level to singles and doubles, the quantum computer

needs to measure the overlaps between excited Slater determinants and the residual vectors, which scales as $O(n_{occ}^2 n_{vir}^2)$. Consequently, the overall shot scaling for these measurements is approximately $O(\eta^4 n_{occ}^2 n_{vir}^2)$. Moreover, the overall shot scaling to construct the matrix M is $O(\eta^4 L^2)$, as we only need to measure the matrix elements within the guess vector subspace instead of all singly and doubly excited determinants. Hence, the primary contribution to the quantum complexities arises from the computations involving the residual vectors. However, with the Davidson method, the dimension of the subspace matrix M is much smaller than that of the full Hamiltonian \tilde{H} , specifically $L \ll n_{occ} n_{vir}$. As a result, the diagonalization step has a computational cost of $O(L^3)$, which is affordable. The Gram–Schmidt procedure determines the cost, which scales as $O(n_{occ}^2 n_{vir}^2 L^2)$. Even this scaling can be further reduced by considering the sparsity and symmetries of the Hamiltonian. In the case of Variational implementation, the classical complexities are not relevant. The primary quantum complexities lie in the measurement of the residual vectors, with an overall shot scaling of approximately $O(\eta^4 n_{occ}^2 n_{vir}^2)$.

III.II. Examples. To illustrate the new algorithms, we consider excited states of four small molecules: $H_2/6-31G$, $H_4/STO-3G$, LiH/STO-3G, and $H_2O/STO-3G$. In H_2O calculations, we use the frozen-core (FC) approximation. The number of qubits for H_2 , H_4 , LiH, and H_2O systems are 8, 8, 12, and 12, respectively. Note that the UCCSD Hamiltonian used in this paper is the same Hamiltonian in the q-sc-EOM approach,⁴⁰ and, therefore, Davidson implementation should yield the identical results. The advantage of the Davidson method is the reduction of the full Hilbert space into a subspace defined by the type and number of target states. Moreover, the q-sc-EOM-UCCSD/Davidson(/Variational) preserves symmetries, i.e., the Davidson routine yields only singlet states if one starts the calculation with the singlet initial guess vectors (subject to numeric noise). Hence, the q-sc-EOM-UCCSD/Davidson(/Variational) computes singlets and triplets separately instead of producing all spin states in one calculation.

Figure 7 shows the potential energy curves of the excited states of four molecules obtained from the q-sc-EOM-UCCSD/Davidson (solid circles) and its variational variant (empty squares) as a function of the bondlengths. The corresponding FCI and q-sc-EOM energies are shown as dashed lines and solid crosses. The absolute errors of the q-sc-EOM-UCCSD/Davidson, Variational, and q-sc-EOM against FCI are shown in the subgraph on top of each panel. The excited states shown in Figure 7 are the four (H_2 , LiH, and H_2O) and five (H_4) lowest-lying excited states for the FCI and q-sc-EOM in the singles and doubles (SD) subspace. In the case of q-sc-EOM-UCCSD/Davidson and Variational, singlet and triplet states are computed separately. As shown in Figure 7, the q-sc-EOM-UCCSD/Davidson and its variational variant reproduce the q-sc-EOM excitation energies for all systems. The excitation energies for $H_2/6-31G$ are identical to the FCI results, showing absolute errors less than 10^{-5} mE_h because the SD level of theory recovers FCI regime for the two-electron systems. The new algorithms also produce nearly exact excitation energies for the LiH/STO-3G system, with errors within the shaded region (MAX(error) ~ 0.17 and ~ 0.30 mE_h for the nonvariational and variational variants, respectively). Figure 7b,d clearly shows that the errors in excitation energies exceed the target accuracy, 1.6 mE_h, for $H_4/STO-3G$ and $H_2O/STO-3G$ at certain internuclear

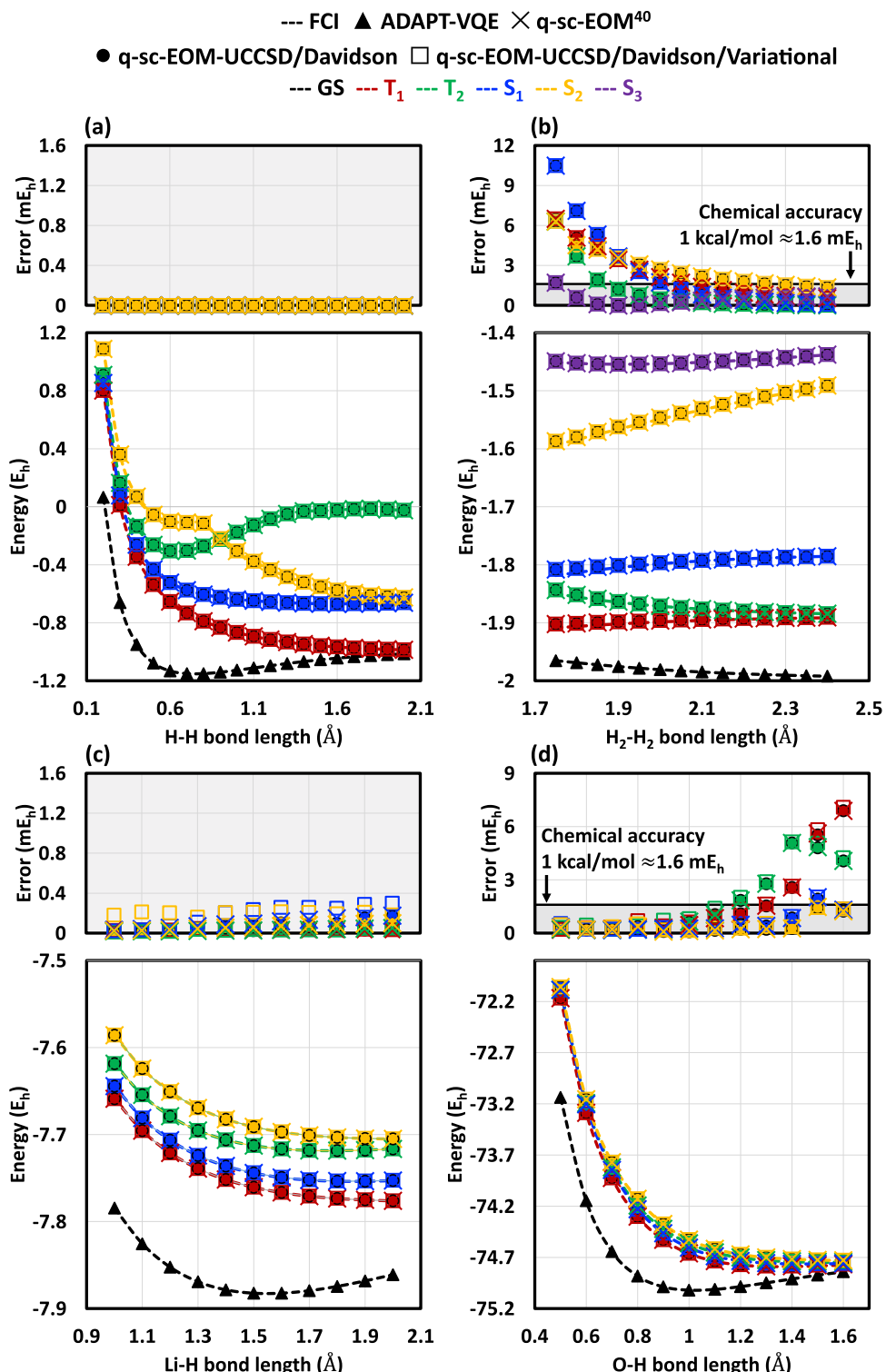


Figure 7. Excitation energies (singlet S and triplet T) for (a) H₂, (b) H₄, (c) LiH, and (d) H₂O as a function of bondlength. The errors with respect to the FCI results are shown in the upper panel, where the shaded region indicates errors below the chemical accuracy of 1 kcal/mol \approx 1.6 mE_h.

distances due to the strong electron correlation—it is well known that triple and higher excitations are significant in the bond-breaking regime.⁸⁷ In the case of the H₄/STO-3G system, one needs to take into account triple excitations for T₁, T₂, S₂, and S₃ states. In addition, even quadruple level of excitations (FCI level) need to be considered to achieve the target accuracy for S₁ in H₄/STO-3G. In this regard, the H₄/STO-3G and H₂O/STO-3G examples illustrate the advantage of using the Davidson

algorithm within q-sc-EOM-UCCSD. Both qEOM³² and q-sc-EOM⁴⁰ diagonalize the entire Hamiltonian within the chosen excitation space—hence, the dimension of the matrix (size of Hilbert space) to diagonalize increases from 26 \times 26 (SD) to 35 \times 35 (SDTQ) for H₄/STO-3G and and 92 \times 92 (SD) to 188 \times 188 (SDT) for H₂O/STO-3G/FC. However, the Davidson algorithm allows one to work with a much smaller subspace, yielding the electronic configurations that are expected to

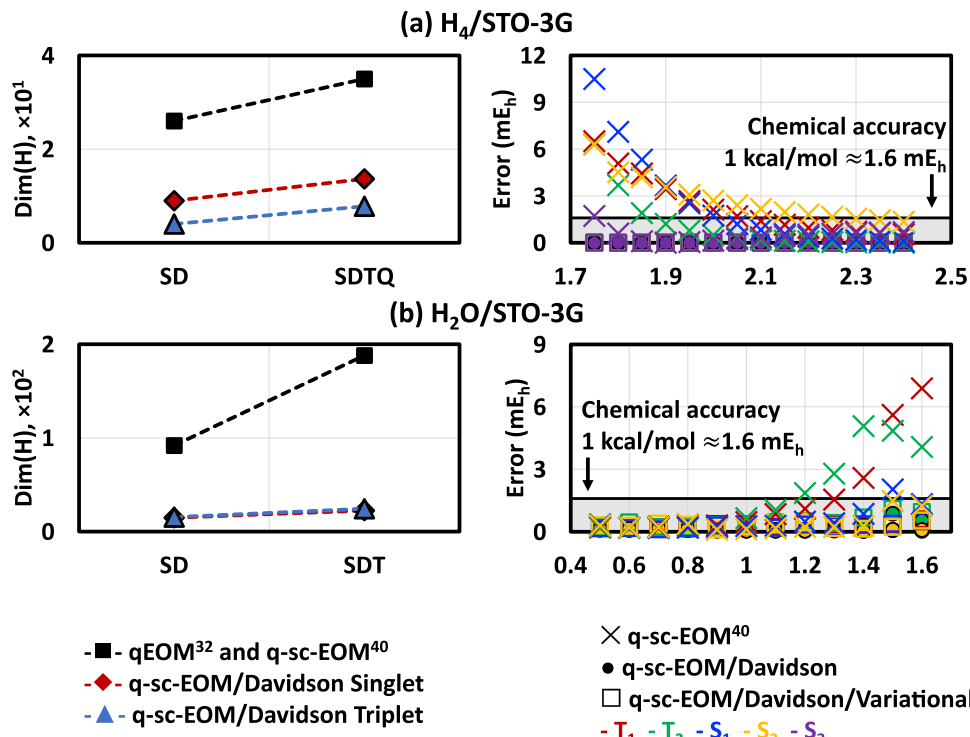


Figure 8. Changes in the dimension of the working pace and the errors with respect to the FCI for (a) H_4 with SDTQ and (b) H_2O with SDT where the shaded region indicates errors below the chemical accuracy of 1 kcal/mol $\approx 1.6 \text{ mE}_h$.

recover the electronic correlations of the current excited state. That is, the dimension of the working space remains within a practical regime for classical computers. The numerical example of $\text{H}_4/\text{STO-3G}$ with SDTQ level of excitations is shown in Figure 8.

Although the dimension of the working space does not grow significantly with the Davidson method, the increase in the level of excitations leads to the increase in the number of projections to be measured in the residual vector calculations of eq 29 (and individual projection should be done with multiple quantum measurements). For example, in the singles and doubles subspace, the number of projections is 26. This number increases to 35 once the quadruple excitations are included. However, quantum measurement processes can be executed in parallel, as shown in the flowcharts in Figures 5 and 6. As long as the scaling for the projection evaluation is not that burdensome, it is a huge advantage.

IV. SUMMARY AND CONCLUSIONS

In this contribution, we discussed the adaptation of the Davidson algorithm to quantum algorithms and presented its implementation within the quantum version of EOM-CC for computing electronically excited states. We tested the method, named q-sc-EOM-UCCSD/Davidson and q-sc-EOM-UCCSD/Davidson/Variational, on four systems: $\text{H}_2/6-31\text{G}$, $\text{H}_4/\text{STO-3G}$, $\text{LiH}/\text{STO-3G}$, and $\text{H}_2\text{O}/\text{STO-3G}(\text{FC})$. The results agree well with the energies obtained from q-sc-EOM.⁴⁰

The Davidson implementation of the q-sc-EOM-UCCSD algorithm provides the advantage over qEOM and q-sc-EOM by reducing the working Hilbert space significantly. The classic Davidson method iteratively interacts with the outcome from the quantum devices and provides feedback for growing the ansatz (vector space) to prepare the desired quantum states. The implementation provides several advantages compared to the

currently available excited-state methods in quantum computing. First, q-sc-EOM-UCCSD/Davidson significantly reduces the computational demand for the classical diagonalization step because the dimension of the resulting subspace Hamiltonian only spanned by a few guess vectors. In the case of its variational variant, the Davidson algorithm provides certain electronic configurations that are expected to contribute to the target excited states. Therefore, it employs a significantly smaller number of variational parameters resulting in a significantly reduced searching space. In addition, similar to the classical variant, the presented Davidson algorithm produces the excited state of the desired spatial or spin symmetry (in the case of the closed-shell references). The q-sc-EOM-UCCSD/Davidson can target the specific group of transitions by defining suitable subspace vectors and can be extended to target higher-energy states or specific transitions.⁴⁴ Apart from the advantages of using the Davidson implementation, the q-sc-EOM-UCCSD shares the key features with the classical EOM-CCSD method except for the form of effective Hamiltonian, such that the different types of excitation variants, such as EA, IP, and SF, can be implemented.

The current NISQ devices are noisy and prohibitively costly in terms of scaling up. They are far from achieving quantum supremacy for quantum-chemistry applications. Hence, efforts have been focused on developing efficient quantum algorithms that combine classical and quantum algorithms, with the hope to gain an advantage, or perhaps just a minor benefit, by leveraging the two technologies. In order to make such hybrid calculations practical, it is essential to reduce the resource requirements for both classical and quantum devices. The essential feature of the Davidson algorithm is the ability to encode a specific linear combination of Slater determinants. To achieve this goal, we used multiqubit controlled gates giving rise to numerous CNOT gates by gate decomposition. Our future work will aim at an

efficient circuit design to reduce the circuit depth and the number of CNOT gates without compromising the stability and accuracy of q-sc-EOM-UCCSD/Davidson and q-sc-EOM-UCCSD/Davidson/Variational.

AUTHOR INFORMATION

Corresponding Authors

Anna I. Krylov – Department of Chemistry, University of Southern California, Los Angeles, California 90089-0482, United States; orcid.org/0000-0001-6788-5016; Email: krylov@usc.edu

Yongbin Kim – Department of Chemistry, University of Southern California, Los Angeles, California 90089-0482, United States; orcid.org/0000-0003-0744-1207; Email: yongbink@usc.edu

Complete contact information is available at:

<https://pubs.acs.org/10.1021/acs.jpca.3c02480>

Notes

The authors declare the following competing financial interest(s): A.I.K. is the president and a part-owner of Q-Chem, Inc.

ACKNOWLEDGMENTS

This work was supported by the Department of Energy award DE-SC0019432. The authors thank Dr. Rosa Di Felice for helpful discussions. The authors are also grateful to Prof. Lan Cheng from the Johns Hopkins University and Prof. Nicholas Mayhall and Dr. Ayush Asthana from Virginia Tech for their valuable feedback about the manuscript.

REFERENCES

- (1) Feynman, R. P. Simulating physics with computers. *Int. J. Theor. Phys.* **1982**, *21*, 467–488.
- (2) Shor, P. W. Polynomial-time algorithms for prime factorization and discrete logarithms on a quantum computer. *SIAM Rev.* **1999**, *41*, 303–332.
- (3) Preskill, J. Quantum computing in the NISQ era and beyond Quantum. *Quantum* **2018**, *2*, No. 79.
- (4) Arute, F.; Arya, K.; Babbush, R.; Bacon, D.; Bardin, J. C.; Barends, R.; Biswas, R.; Boixo, S.; Brandao, F. G. S. L.; Buell, D. A.; et al. Quantum supremacy using a programmable superconducting processor. *Nature* **2019**, *574*, 505–510.
- (5) Arute, F.; Arya, K.; Babbush, R.; Bacon, D.; Bardin, J. C.; Barends, R.; Boixo, S.; Broughton, M.; Buckley, B. B.; Buell, D. A.; et al. Hartree-Fock on a superconducting qubit quantum computer. *Science* **2020**, *369*, 1084–1089.
- (6) Krylov, A. I.; Doyle, J.; Ni, K.-K. A preface for a themed PCCP collection on quantum information science. *Phys. Chem. Chem. Phys.* **2021**, *23*, 6341–6343.
- (7) Aspuru-Guzik, A.; Dutoi, A. D.; Love, P. J.; Head-Gordon, M. Simulated quantum computation of molecular energies. *Science* **2005**, *309*, 1704–1707.
- (8) Abrams, D. S.; Lloyd, S. Simulation of many-body fermionic systems on a universal quantum computer. *Phys. Rev. Lett.* **1997**, *79*, 2586–2589.
- (9) Abrams, D. S.; Lloyd, S. Quantum algorithm providing exponential speed increase for finding eigenvalues and eigenvectors. *Phys. Rev. Lett.* **1999**, *83*, 5162–5165.
- (10) Lanyon, B. P.; Whitfield, J. D.; Gillett, G. G.; Goggin, M. E.; Almeida, M. P.; Kissal, I.; Biamonte, J. D.; Mohseni, M.; Powell, B. J.; Barbieri, M.; et al. Towards quantum chemistry on a quantum computer. *Nat. Chem.* **2010**, *2*, 106–111.
- (11) Jones, N. C.; Whitfield, J. D.; McMahon, P. L.; Yung, M.-H.; Meter, R. V.; Aspuru-Guzik, A.; Yamamoto, Y. Faster quantum chemistry simulation on fault-tolerant quantum computers. *New J. Phys.* **2012**, *14*, No. 115023.
- (12) Whitfield, J. D.; Biamonte, J.; Aspuru-Guzik, A. Simulation of electronic structure Hamiltonians using quantum computers. *Mol. Phys.* **2011**, *109*, 735–750.
- (13) Peruzzo, A.; McClean, J.; Shadbolt, P.; Yung, M.-H.; Zhou, X.-Q.; Love, P. J.; Aspuru-Guzik, A.; O'Brien, J. L. A variational eigenvalue solver on a photonic quantum processor. *Nat. Comm.* **2014**, *5*, No. 4213.
- (14) McClean, J. R.; Romero, J.; Babbush, R.; Aspuru-Guzik, A. The theory of variational hybrid quantum-classical algorithms. *New J. Phys.* **2016**, *18*, No. 023023.
- (15) O'Malley, P. J. J.; Babbush, R.; Kivlichan, I. D.; Romero, J.; McClean, J. R.; Barends, R.; Kelly, J.; Roushan, P.; Tranter, A.; Ding, N.; et al. Scalable quantum simulation of molecular energies. *Phys. Rev. X* **2016**, *6*, No. 031007.
- (16) Kandala, A.; Mezzacapo, A.; Temme, K.; Takita, M.; Brink, M.; Chow, J. M.; Gambetta, J. M. Hardware-efficient variational quantum eigensolver for small molecules and quantum magnets. *Nature* **2017**, *549*, 242–246.
- (17) Colless, J. I.; Ramasesh, V. V.; Dahlen, D.; Blok, M. S.; Kimchi-Schwartz, M. E.; McClean, J. R.; Carter, J.; deJong, W. A.; Siddiqi, I. Computation of molecular spectra on a quantum processor with an error-resilient algorithm. *Phys. Rev. X* **2018**, *8*, No. 011021.
- (18) Nam, Y.; Chen, J.-S.; Pisenti, N. C.; Wright, K.; Delaney, C.; Maslov, D.; Brown, K. R.; Allen, S.; Amini, J. M.; Apisdorf, J.; et al. Ground-state energy estimation of the water molecule on a trapped-ion quantum computer. *npj Quantum Inf.* **2020**, *6*, No. 33.
- (19) Higgott, O.; Wang, D.; Brierley, S. Variational quantum computation of excited states. *Quantum* **2019**, *3*, No. 156.
- (20) Nakanishi, K. M.; Mitarai, K.; Fujii, K. Subspace-search variational quantum eigensolver for excited states. *Phys. Rev. Res.* **2019**, *1*, No. 033062.
- (21) Parrish, R. M.; Hohenstein, E. G.; McMahon, P. L.; Martínez, T. J. Quantum computation of electronic transitions using a variational quantum eigensolver. *Phys. Rev. Lett.* **2019**, *122*, No. 230401.
- (22) Ryabinkin, I. G.; Genin, S. N.; Izmaylov, A. F. Constrained variational quantum eigensolver: Quantum computer search engine in the Fock space. *J. Chem. Theory Comput.* **2019**, *15*, 249–255.
- (23) Jones, T.; Endo, S.; McArdle, S.; Yuan, X.; Benjamin, S. C. Variational quantum algorithms for discovering Hamiltonian spectra. *Phys. Rev. A* **2019**, *99*, No. 062304.
- (24) Xie, Q.-X.; Liu, S.; Zhao, Y. Orthogonal state reduction variational eigensolver for the excited-state calculations on quantum computers. *J. Chem. Theory Comput.* **2022**, *18*, 3737–3746.
- (25) Helgaker, T.; Jørgensen, P.; Olsen, J. *Molecular Electronic Structure Theory*; Wiley & Sons, 2000; pp 1–944.
- (26) Dreuw, A.; Head-Gordon, M. Single-reference ab initio methods for the calculation of excited states of large molecules. *Chem. Rev.* **2005**, *105*, 4009–4037.
- (27) Dreuw, A.; Wormit, M. The algebraic diagrammatic construction scheme for the polarization propagator for the calculation of excited states. *Wiley Interdiscip. Rev.: Comput. Mol. Sci.* **2015**, *5*, 82–95.
- (28) Krylov, A. I. Equation-of-motion coupled-cluster methods for open-shell and electronically excited species: The hitchhiker's guide to Fock space. *Annu. Rev. Phys. Chem.* **2008**, *59*, 433–462.
- (29) Bartlett, R. J. The coupled-cluster revolution. *Mol. Phys.* **2010**, *108*, 2905–2920.
- (30) Sneskov, K.; Christiansen, O. Excited state coupled cluster methods. *Wiley Interdiscip. Rev.: Comput. Mol. Sci.* **2012**, *2*, 566–584.
- (31) Bartlett, R. J. Coupled-cluster theory and its equation-of-motion extensions. *Wiley Interdiscip. Rev.: Comput. Mol. Sci.* **2012**, *2*, 126–138.
- (32) Ollitrault, P. J.; Kandala, A.; Chen, C.-F.; Barkoutsos, P. K.; Mezzacapo, A.; Pistoia, M.; Sheldon, S.; Woerner, S.; Gambetta, J. M.; Tavernelli, I. Quantum equation of motion for computing molecular excitation energies on a noisy quantum processor. *Phys. Rev. Res.* **2020**, *2*, No. 043140.

- (33) Fan, Y.; Liu, J.; Li, Z.; Yang, J. Equation-of-motion theory to calculate accurate band structures with a quantum computer. *J. Phys. Chem. Lett.* **2021**, *12*, 8833–8840.
- (34) Pavošević, F.; Hammes-Schiffer, S. Multicomponent unitary coupled cluster and equation-of-motion for quantum computation. *J. Chem. Theory Comput.* **2021**, *17*, 3252–3258.
- (35) Romero, J.; Babbush, R.; McClean, J. R.; Hempel, C.; Love, P. J.; Aspuru-Guzik, A. Strategies for quantum computing molecular energies using the unitary coupled cluster ansatz. *Quantum Sci. Technol.* **2019**, *4*, No. 014008.
- (36) Szekeres, Z.; Szabados, Á.; Kállay, M.; Surján, P. R. On the “killer condition” in the equation-of-motion method: Ionization potentials from multi-reference wave functions. *Phys. Chem. Chem. Phys.* **2001**, *3*, 696–701.
- (37) Prasad, M. D.; Pal, S.; Mukherjee, D. Some aspects of self-consistent propagator theories. *Phys. Rev. A* **1985**, *31*, 1287–1298.
- (38) Levchenko, S. V.; Krylov, A. I. Equation-of-motion spin-flip coupled-cluster model with single and double substitutions: Theory and application to cyclobutadiene. *J. Chem. Phys.* **2004**, *120*, 175–185.
- (39) Datta, B.; Mukhopadhyay, D.; Mukherjee, D. Consistent propagator theory based on the extended coupled-cluster parametrization of the ground state. *Phys. Rev. A* **1993**, *47*, 3632–3648.
- (40) Asthana, A.; Kumar, A.; Abraham, V.; Grimsley, H.; Zhang, Y.; Cincio, L.; Tretiak, S.; Dub, P. A.; Economou, S. E.; Barnes, E.; Mayhall, N. J. Quantum self-consistent equation-of-motion method for computing molecular excitation energies, ionization potentials, and electron affinities on a quantum computer. *Chem. Sci.* **2023**, *14*, 2405–2418.
- (41) Davidson, E. R. The iterative calculation of a few of the lowest eigenvalues and corresponding eigenvectors of large real-symmetric matrices. *J. Comput. Phys.* **1975**, *17*, 87–94.
- (42) Hirao, K.; Nakatsuji, H. A generalization of the Davidson’s method to large nonsymmetric eigenvalue problems. *J. Comput. Phys.* **1982**, *45*, 246–254.
- (43) Rettrup, S. An iterative method for calculating several of the extreme eigensolutions of large real non-symmetric matrices. *J. Comput. Phys.* **1982**, *45*, 100–107.
- (44) Zuev, D.; Vecharynski, E.; Yang, C.; Orms, N.; Krylov, A. I. New algorithms for iterative matrix-free eigensolvers in quantum chemistry. *J. Comput. Chem.* **2015**, *36*, 273–284.
- (45) Nielsen, M. A.; Chuang, I. L. *Quantum Computation and Quantum Information: 10th Anniversary Edition*; Cambridge University Press, 2010; pp 1–702.
- (46) Gard, B. T.; Zhu, L.; Barron, G. S.; Mayhall, N. J.; Economou, S. E.; Barnes, E. Efficient symmetry-preserving state preparation circuits for the variational quantum eigensolver algorithm. *npj Quantum Inf.* **2020**, *6*, No. 10.
- (47) Rowe, D. J. Equations-of-motion method and the extended shell model. *Rev. Mod. Phys.* **1968**, *40*, 153–166.
- (48) McCurdy, C. W.; Rescigno, T. N.; Yeager, D. L.; McKoy, V. *Methods of Electronic Structure Theory*; Plenum Press: New York, 1977; Vol. 3, p 339.
- (49) McKoy, V. The equations of motion method: An approach to the dynamical properties of atoms and molecules. *Phys. Scr.* **1980**, *21*, 238–241.
- (50) McWeeny, R. *Methods of Molecular Quantum Mechanics*, 2nd ed.; Academic Press, 1992.
- (51) Manne, R. A completeness theorem for operator spaces. *Chem. Phys. Lett.* **1977**, *45*, 470–472.
- (52) Dalgaard, E. Expansion and completeness theorems for operator manifolds. *Int. J. Quantum Chem.* **1979**, *15*, 169–180.
- (53) Čížek, J. On the correlation problem in atomic and molecular systems. Calculation of wavefunction components in Ursell-type expansion using quantum-field theoretical methods. *J. Chem. Phys.* **1966**, *45*, 4256–4266.
- (54) Čížek, J.; Paldus, J. Correlation problems in atomic and molecular systems iii. rederivation of the coupled-pair many-electron theory using the traditional quantum chemical methodst. *Int. J. Quantum Chem.* **1971**, *5*, 359–379.
- (55) Crawford, T. D.; Schaefer, H. F., III An Introduction to Coupled Cluster Theory for Computational Chemists. In *Reviews in Computational Chemistry*; John Wiley & Sons, 2000; Vol. 14, pp 33–136.
- (56) Bartlett, R. J.; Shavitt, I. *Many-Body Methods in Chemistry and Physics: MBPT and Coupled-Cluster Theory*; Cambridge University Press, 2009; pp 1–532.
- (57) Emrich, K. An extension of the coupled-cluster formalism to excited states (I). *Nucl. Phys. A* **1981**, *351*, 379–396.
- (58) Sekino, H.; Bartlett, R. J. A linear response, coupled-cluster theory for excitation energy. *Int. J. Quantum Chem.* **1984**, *26*, 255–265.
- (59) Comeau, D. C.; Bartlett, R. J. The equation-of-motion coupled-cluster method. Applications to open- and closed-shell reference states. *Chem. Phys. Lett.* **1993**, *207*, 414–423.
- (60) Stanton, J. F.; Bartlett, R. J. The equation of motion coupled-cluster method. A systematic biorthogonal approach to molecular excitation energies, transition probabilities, and excited state properties. *J. Chem. Phys.* **1993**, *98*, 7029–7039.
- (61) Van Voorhis, T.; Head-Gordon, M. Benchmark variational coupled-cluster results. *J. Chem. Phys.* **2000**, *113*, 8873–8879.
- (62) Taube, A. G.; Bartlett, R. J. New perspectives on unitary coupled-cluster theory. *Int. J. Quantum Chem.* **2006**, *106*, 3393–3401.
- (63) Liu, J.; Asthana, A.; Cheng, L.; Mukherjee, D. Unitary coupled-cluster based self-consistent polarization propagator theory: A third-order formulation and pilot applications. *J. Chem. Phys.* **2018**, *148*, No. 244110.
- (64) Liu, J.; Cheng, L. Unitary coupled-cluster based self-consistent polarization propagator theory: A quadratic unitary coupled-cluster singles and doubles scheme. *J. Chem. Phys.* **2021**, *155*, No. 174102.
- (65) Liu, J.; Matthews, D. A.; Cheng, L. Quadratic unitary coupled-cluster singles and doubles scheme: Efficient implementation, benchmark study, and formulation of an extended version. *J. Chem. Theory Comput.* **2022**, *18*, 2281–2291.
- (66) Trotter, H. F. On the product of semi-groups of operators. *Proc. Am. Math. Soc.* **1959**, *10*, 545–551.
- (67) Suzuki, M. General decomposition theory of ordered exponentials. *Proc. Jpn. Acad., Ser. B* **1993**, *69*, 161–166.
- (68) Jordan, P.; Wigner, E. P. *Über das Paulische Äquivalenzverbot*; Springer: Berlin Heidelberg, 1993; pp 109–129.
- (69) Ortiz, G.; Gubernatis, J. E.; Knill, E.; Laflamme, R. Quantum algorithms for fermionic simulations. *Phys. Rev. A* **2001**, *64*, No. 022319.
- (70) Yung, M.-H.; Casanova, J.; Mezzacapo, A.; McClean, J.; Lamata, L.; Aspuru-Guzik, A.; Solano, E. From transistor to trapped-ion computers for quantum chemistry. *Sci. Rep.* **2014**, *4*, No. 3589.
- (71) Wang, D.; Higgott, O.; Brierley, S. Accelerated variational quantum eigensolver. *Phys. Rev. Lett.* **2019**, *122*, No. 140504.
- (72) Leon, S. J.; Björck, Å.; Gander, W. Gram-Schmidt orthogonalization: 100 years and more. *Numer. Linear Algebra Appl.* **2013**, *20*, 492–532.
- (73) McClean, J. R.; Rubin, N.; Sung, K. J.; Kivlichan, I. D.; Bonet-Monroig, X.; Cao, Y.; Dai, C.; Fried, E. S.; Gidney, C.; Gimby, B.; et al. OpenFermion: the electronic structure package for quantum computers. *Quantum Sci. Technol.* **2020**, *5*, No. 034014.
- (74) Kim, Y.; Epifanovsky, E.; Krylov, A. I. Openfermion/Q-Chem Interface, 2023. <https://github.com/qchemsoftware/OpenFermion-QChem>. (accessed June 19, 2023).
- (75) Qiskit: An open-source framework for quantum computing. Qiskit contributors, 2023. <https://github.com/Qiskit/qiskit-terra/blob/main/CITATION.bib>. (accessed June 19, 2023).
- (76) Buhrman, H.; Cleve, R.; Watrous, J.; deWolf, R. Quantum fingerprinting. *Phys. Rev. Lett.* **2001**, *87*, No. 167902.
- (77) Gottesman, D.; Chuang, I. L. Quantum digital signatures, arXiv:0105032. arXiv.org e-Print archive. <https://doi.org/10.48550/arXiv.quant-ph/0105032>, 2001.
- (78) Garcia-Escartin, J. C.; Chamorro-Posada, P. SWAP test and Hong-Ou-Mandel effect are equivalent. *Phys. Rev. A* **2013**, *87*, No. 052330.

- (79) Huggins, W. J.; Lee, J.; Baek, U.; O'Gorman, B.; Whaley, K. B. A non-orthogonal variational quantum eigensolver. *New J. Phys.* **2020**, *22*, No. 073009.
- (80) McClean, J. R.; Boixo, S.; Smelyanyky, V. N.; Babbush, R.; Neven, H. Barren plateaus in quantum neural network training landscapes. *Nat. Commun.* **2018**, *9*, No. 4812.
- (81) Grimsley, H. R.; Economou, S. E.; Barnes, E.; Mayhall, N. J. An adaptive variational algorithm for exact molecular simulations on a quantum computer. *Nat. Commun.* **2019**, *10*, No. 3007.
- (82) Kim, Y.; Krylov, A. I. qeom-ucc/davidson, 2023. <https://github.com/yongbinkim-chemist/qEOM-UCC>. (accessed June 19, 2023).
- (83) Epifanovsky, E.; Gilbert, A. T. B.; Feng, X.; Lee, J.; Mao, Y.; Mardirossian, N.; Pokhilko, P.; White, A. F.; Coons, M. P.; Dempwolff, A. L.; et al. Software for the frontiers of quantum chemistry: An overview of developments in the Q-Chem 5 package. *J. Chem. Phys.* **2021**, *155*, No. 084801.
- (84) Asthana, A.; Kumar, A.; Grimsley, H. R.; Mayhall, N. J. Adapt-VQE, 2023. <https://github.com/asthanaa/adapt-vqe>. (accessed June 19, 2023).
- (85) Virtanen, P.; Gommers, R.; Oliphant, T. E.; Haberland, M.; Reddy, T.; Cournapeau, D.; Burovski, E.; Peterson, P.; Weckesser, W.; Bright, J.; et al. Scipy 1.0: fundamental algorithms for scientific computing in python. *Nat. Methods* **2020**, *17*, 261–272.
- (86) Cirq. Developers, Cirq, 2022. <https://github.com/quantumlib/Cirq/graphs/contributors>. (accessed June 19, 2023).
- (87) Li, X.; Paldus, J. Performance of multireference and equation-of-motion coupled-cluster methods for potential energy surfaces of low-lying excited states: Symmetric and asymmetric dissociation of water. *J. Chem. Phys.* **2010**, *133*, No. 024102.